(FBS) and 100 U/mL penicillin–streptomycin in 5% CO_2 at 37 °C. Cells were maintained at a density of 60%–70% confluence in 100 mm dishes, and used in log-phase of growth.

3.4. Characterization of MgNP-Fe_3O_4 Suspensions in Cell Culture Medium

The average hydrodynamic size and size distribution of MgNPs-Fe_3O_4 in cell culture media and their intracellular localization were determined by DLS using a Fiber-Optics Particle Analyzer FPAR-1000 (Otsuka Electronics, Hirakata, Osaka, Japan). MgNPs-Fe_3O_4 were suspended in Ham's F-12 Medium with or without 10% FBS and supplements, or in phosphate-buffered saline (PBS).

3.5. Cellular Uptake of MgNPs-Fe_3O_4 in A549 Cells

The cellular uptake of MgNPs-Fe_3O_4 in A549 cells was analyzed as follows.

3.5.1. Transmission Electron Microscopy (TEM)

A549 cells were fixed with 3% glutaraldehyde in 0.1 M cacodylate buffer (pH 7.3) at 4 °C for 4 h. Samples were post-fixed with 2% osmium tetraoxide at 4 °C for 2 h, dehydrated, and embedded in epoxy resin. Ultrathin sections (80 nm) were then stained with uranyl acetate and lead citrate, and observed by TEM.

3.5.2. Flow Cytometry Assay

A549 cells were treated with 0, 1, 10 or 100 μg/mL MgNPs-Fe_3O_4 for 24 h, and then trypsinized and suspended in medium. Cellular uptake of MgNPs-Fe_3O_4 was analyzed using flow cytometry (Millipore, Billerica, MA, USA), in which the intensities of forward-scattered (FS) and side-scattered (SS) light are proportional to cell size and intracellular density of MgNPs-Fe_3O_4, respectively. A total of 30,000 cells were measured per sample.

3.6. AlamarBlue Assay

Cell viability was determined using the alamarBlue assay (Alamar Biosciences, Sacramento, California, USA) according to the manufacturer's instructions. Briefly, cells (1.0×10^4 cells/well) were incubated with MgNPs-Fe_3O_4 (0, 1, 10 or 100 μg/mL) for 72 h at 37 °C. AlamarBlue (10%) was added to each well and incubated for 200 min. Metabolically active cells reduced the dye to a fluorescent form, which was measured using a plate reader (excitation/emission: 570 nm/600 nm; Viento XS, DS Pharma Biomedical, Suita, Osaka, Japan). Cell viability was determined by linear interpolation of the emission from cells treated with 0.1% saponin (0% viability) and untreated cells (100% viability).

3.7. Lactate Dehydrogenase (LDH) Release Assay

LDH release assay to assess membrane integrity was performed using LDH-cytotoxicity assay kit (BioVision, CA, USA) according to the manufacturer's instructions. Cells cultured in 24-well plates (1.5×10^4 cells/well) were treated with 0, 1, 10 or 100 μg/mL MgNPs-Fe_3O_4 for 24 h at 37 °C. Plates were then centrifuged at 250× *g* for 5 min. The supernatant of each well was transferred to a fresh, flat

bottom 96-well culture plate containing 100 μL reaction mixture, and incubated for 30 min at room temperature. Formazan absorbance—an index of the number of lysed cells—was measured by a microplate reader at 500 nm (Viento XS, DS Pharma Biomedical, Osaka, Japan).

3.8. Apoptosis by Flow Cytometry (FCM)

A549 cells (1.0×10^6 cells) were cultured on 100-mm culture dishes, and treated with 0, 1, 10 or 100 μg/mL MgNPs-Fe_3O_4 for 24 h at 37 °C. Cells were harvested, washed gently with PBS, collected by centrifugation, and then stained using an Annexin V-FITC Kit (Beckman Coulter, Marseille, France) following the manufacturer's instructions. Cells were stained with Annexin V and propidium iodide (PI, Sigma-Aldrich, St. Louis, MO, USA), and analyzed by flow cytometry (Becton Dickinson, Franklin Lakes, NJ, USA) within 1 h of staining using the FL1 (FITC) and FL3 (PI) lines.

3.9. Measurement of Intracellular Reactive Oxygen Species (ROS)

ROS were measured using the CM-H_2DCFDA assay (Invitrogen, Carlsbad, CA, USA) according to the manufacturer's instructions. Cells (1.0×10^4 cells/well) in 24 well-plates were treated with 0, 1, 10 or 100 μg/mL MGNPs-Fe_3O_4 for 24 h at 37 °C. A fresh stock solution of 5 mM CM-H_2DCFDA was prepared in DMSO and diluted to a final concentration of 1 μM in PBS. Cells were washed with PBS, followed by incubation with 50 μL of working solution of the fluorochrome marker CM-H_2 DCFDA for 30 min. Fluorescent images were obtained using an IX2N-FL-1 microscope (Olympus, Tokyo, Japan), and analyzed using imaging soft (Photoshop Elements 8, Adobe systems, Tokyo, Japan). The data were expressed as percentage of the unexposed control.

3.10. Intracellular Reduced Glutathione (GSH) Assay

Intracellular GSH level was determined using a GSH-Glo Glutathione assay kit (Promega, Madison, WI, USA) according to the manufacturer's instructions. Briefly, cells were seeded in 96-well plates and treated with 0, 1, 10 or 100 μg/mL MgNPs-Fe_3O_4 for 24 h at 37 °C. The cells were washed with DPBS, and the GSH-Glo reagent was added to each well for 30 min at room temperature to allow the cells to convert a luciferin derivative into luciferin. Reconstituted luciferin detection reagent was then added to each well for 15 min, and the luminescent signal was measured with a Glomax multi detection system (Promega, Madison, WI, USA).

3.11. Analysis of 8-Hydroxy-2'-Deoxyguanosine (8-OH-dG) in DNA

A549 cells were incubated with 0, 1, 10 or 100 μg/mL MGNPs-Fe_3O_4 for 72 h at 37 °C (5% CO_2). The nuclear DNA was isolated by the sodium iodide method. The 8-OH-dG levels were analyzed by HPLC-ECD methods as previously described [27]. The amount of 8-OH-dG in the DNA was determined by comparison to authentic standards, and expressed as the number of 8-OH-dG per 10^6 deoxyguanosine (dG) residues.

3.12. Oxidative Stress-Related Gene Expression Analysis

A549 cells were treated with 0, 1, 10, or 100 μg/mL MgNPs-Fe_3O_4 for 24 h at 37 °C. Total RNA was isolated using ISOGEN (Nippon Gene, Tokyo, Japan), and cDNA was produced using a mixture containing Superscript RNase H Reverse Transcriptase (Invitrogen, Carlsbad, CA, USA), oligo dT primer, and 2.5 mmol/L dNTP. Quantitative real-time PCR was conducted using the LINE GENE real-time PCR detection system (BioFlux, Tokyo, Japan) with the SYBR Premix Ex Taq Perfect Real Time Kit (Takara Bio. Inc., Otsu, Japan). The PCR reaction consisted of initial thermal activation at 95 °C for 10 s and 40 cycles. Each cycle was as follows: 95 °C for 5 s; 60 °C for 26 s. PCR producs were verified by analysis of heat-dissociation curves and amplification plots. Quantitative values were acquired from linear regression of the PCR standard curve. The primer sequences of the amplified genes are as follows [28,29]; *Heme oxygenase-1*, forward 5'-GGTGATAGAAGAGGCCAAGAC-3' and reverse 5'-GCAGAATCTTGCACTTTGTTG-3', β-*actin*, forward 5'-GGATGCAGAAGG AGATCACTG-3' and reverse 5'-CGATCCACACGGAGTACTTG-3'.

3.13. Immunostaining and Flow Cytometric Analysis for $CD44^+$ Cell Fraction

A549 cells were treated with 0, 1, 10 or 100 μg/mL MgNPs-Fe_3O_4 for 24 h at 37 °C. Cells were then labeled in a PBS solution with a mouse anti-human CD44 monoclonal antibody conjugated with fluorescein isothiocyanate (clone SFF-2, Millipore, Billerica, MA, USA) for 1 h at room temperature. A mouse IgG immunoglobulin and dye conjugate IgG was used as control for non-specific binding. Flow cytometric analysis was performed with a Guava-EasyCyte*HT using Guava Express Pro software (Millipore, Billerica, MA, USA) gating for $CD44^+$ cells. A minimum of 10,000 cells was measured per sample.

3.14. Statistical Analysis

Data are presented as the mean ± standard deviation (SD). Differences between treated and untreated control cells were determined using one-way ANOVA followed by Dunnett's test. Differences were considered statistically significant at $p < 0.05$.

4. Conclusions

MgNPs-Fe_3O_4 up to a concentration of 100 μg/mL exerted minimal effect on viability of A549 cells, despite causing a significant reduction in antioxidant capacity and an increase in oxidative damage to DNA. Increased expression of an oxidative stress-related gene was not sufficient to prevent the decrease in GSH content. The decrease in the $CD44^+$ cell fraction was consistent with the observed drop in GSH concentration and increase in 8-OH-dG level.

Acknowledgments

This research was supported in part by a Grant-in-Aid for the Global COE Program from the Ministry of Education, Culture, Sports, Science and Technology of Japan, a Grant-in-Aid for Research

on Risk of Chemical Substances from the Ministry of Health, Labour and Welfare of Japan, and a Research Grand-in-Aid from Magnetic Health Science Foundation.

Conflict of Interest

The authors report no conflict of interest. The authors are responsible for the content and writing of the paper.

References

1. Chakraborty, M.; Jain, S.; Rani, V. Nanotechnology: Emerging tool for diagnostics and therapeutics. *Appl. Biochem. Biotechnol.* **2011**, *165*, 1178–1187.
2. Ramesh, V.; Ravichandran, P.; Copeland, C.L.; Gopikrishnan, R.; Biradar, S.; Goornavar, V.; Ramesh, G.T.; Hall, J.C. Magnetite induces oxidative stress and apoptosis in lung epithelial cells. *Mol. Cell. Biochem.* **2012**, *363*, 225–234.
3. Parveen, S.; Misra, R.; Sahoo, S.K. Nanoparticles: A boon to drug delivery, therapeutics, diagnostics and imaging. *Nanomedicine* **2012**, *8*, 147–166.
4. Hilger, I.; Kaiser, W.A. Iron oxide-based nanostructures for MRI and magnetic hyperthermia. *Nanomedicine* **2012**, *7*, 1443–1459.
5. Chen, B.; Sun, Q.; Wang, X.; Gao, F.; Dai, Y.; Yin, Y.; Ding, J.; Gao, C.; Cheng, J.; Li, J.; *et al.* Reversal in multidrug resistance by magnetic nanoparticle of Fe_3O_4 loaded with adriamycin and tetrandrine in K562/A02 leukemic cells. *Int. J. Nanomed.* **2008**, *3*, 277–286.
6. Sato, A.; Itcho, N.; Ishiguro, H.; Okamoto, D.; Kawai, K.; Kasai, H.; Kurioka, D.; Uemura, H.; Kubota, Y.; Watanabe, M. Magnetic nanoparticles of Fe_3O_4 enhance docetaxel-induced prostate cancer cell death. *Int. J. Nanomed.* **2013**, in press.
7. Singh, N.; Jenkins, G.J.; Asadi, R.; Doak, S.H. Potential toxicity of superparamagnetic iron oxide nanoparticles (SPION). *Nano Rev.* **2010**, *1*, 5358.
8. Karlsson, H.L.; Cronholm, P.; Gustafsson, J.; Möller, L. Copper oxide nanoparticles are highly toxic: A comparison between metal oxide nanoparticles and carbon nanotubes. *Chem. Res. Toxicol.* **2008**, *21*, 1726–1732.
9. Kim, J.E.; Shin, J.Y.; Cho, M.H. Magnetic nanoparticles: An update of application for drug delivery and possible toxic effects. *Arch. Toxicol.* **2012**, *86*, 685–700.
10. Lewinski, N.; Colvin, V.; Drezek, R. Cytotoxicity of nanoparticles. *Small* **2008**, *4*, 26–49.
11. Klein, S.; Sommer, A.; Distel, L.V.; Neuhuber, W.; Kryschi, C. Superparamagnetic iron oxide nanoparticles as radiosensitizer via enhanced reactive oxygen species formation. *Biochem. Biophys. Res. Commun.* **2012**, *425*, 393–397.
12. Holgate, S.T. Epithelial damage and response. *Clin. Exp. Allergy.* **2000**, *1*, 37–41.
13. Kitamura, H.; Okudela, K.; Yazawa, T.; Sato, H.; Shimoyamada, H. Cancer stem cell: Implications in cancer biology and therapy with special reference to lung cancer. *Lung Cancer* **2009**, *66*, 275–281.
14. Hong, S.C.; Lee, J.H.; Kim, H.Y.; Park, J.Y.; Cho, J.; Lee, J.; Han, D.W. Subtle cytotoxicity and genotoxicity differences in superparamagnetic iron oxide nanoparticles coated with various functional groups. *Int. J. Nanomed.* **2011**, *6*, 3219–3231.

15. Wiogo, H.T.R.; Lim, M.; Bulmus, V.; Yun, J.; Amal, R. Stabilization of magnetic iron oxide nanoparticles in biological media by fetal bovine serum (FBS). *Langmuir* **2011**, *27*, 843–850.
16. Birben, E.; Sahiner, U.M.; Sackesen, C.; Erzurum, S.; Kalayci, O. Oxidative stress and antioxidant defense. *World Allergy Organ J.* **2012**, *5*, 9–19.
17. Tulis, D.A.; Durante, W.; Liu, X.; Evans, A.; Peyton, K.J.; Schafer, A.I. Adenovirus-mediated heme oxygenase-1 gene delivery inhibits injury-induced vascular neointima formation. *Circulation* **2001**, *104*, 2710–2715.
18. Morita, T. Heme oxygenase and atherosclerosis. *Thromb. Vasc. Biol.* **2005**, *25*, 1786–1795.
19. Durante, W. Heme oxygenase-1 in growth control and its clinical application to vascular disease. *J. Cell Physiol.* **2003**, *195*, 373–382.
20. Park, E.J.; Yi, J.; Chung, K.H.; Ryu, D.Y.; Choi, J.; Park, K. Oxidative stress and apoptosis induced by titanium dioxide nanoparticles in cultured BEAS-2B cells. *Toxicol. Lett.* **2008**, *180*, 222–229.
21. Napierska, D.; Rabolli, V.; Thomassen, L.C.J.; Dinsdale, D.; Princen, C.; Gonzalez, L.; Poels, K.L.C.; Kirsch-Volders, M.; Lison, D.; Martens, J.A.; *et al.* Oxidative stress induced by pure and iron-doped amorphous silica nanoparticles in subtoxic conditions. *Chem. Res. Toxicol.* **2012**, *25*, 828–837.
22. Yasuda, M.; Nakano, K.; Yasumoto, K.; Tanaka, Y. CD44: Functional relevance to inflammation and malignancy. *Histol. Histopathol.* **2002**, *17*, 945–950.
23. Leir, S.H.; Baker, J.E.; Holgate, S.T.; Lackie, P.M. Increased CD44 expression in human bronchial epithelial repair after damage or plating at low cell densities. *Am. J. Physiol. Lung Cell Mol. Physiol.* **2000**, *278*, L1129–L1137.
24. Leung, E.L.; Fiscus, R.R.; Tung, J.W.; Tin, V.P.; Cheng, L.C.; Sihoe, A.D.; Fink, L.M.; Ma, Y.; Wong, M.P. Non-small cell lung cancer cells expressing CD44 are enriched for stem cell-like properties. *PLoS One* **2010**, *5*, e14062.
25. Nagano, O.; Okazaki, S.; Saya, H. Redox regulation in stem-like cancer cells by CD44 variant isoforms. *Oncogene* **2013**, in press.
26. Zhao, H.; Tanaka, T.; Mitlitski, V.; Heeter, J, Balazs, E.A.; Darzynkiewicz, Z. Protective effect of hyaluronate on oxidative DNA damage in WI-38 and A549 cells. *Int. J. Oncol.* **2008**, *32*, 1159–1167.
27. Kawai, K.; Li, Y.S.; Kasai, H. Accurate measurement of 8-OH-dG and 8-OH-Gua in mouse DNA, urine and serum: Effects of X-ray irradiation. *Genes Environ.* **2007**, *29*, 107–114.
28. Miyake, M.; Fujimoto, K.; Anai, S.; Ohnishi, S.; Kuwada, M.; Nakai, Y.; Inoue, T.; Matsumura, Y.; Tomioka, A.; Ikeda, T.; *et al.* Heme oxygenase-1 promotes angiogenesis in urothelial carcinoma of the urinary bladder. *Oncol. Rep.* **2011**, *25*, 653–660.
29. Wang, C.; Tian, Y.; Lei, B.; Xiao, X.; Ye, Z.; Li, F.; Kijlstra, A.; Yang, P. Decreased IL-27 expression in assiciation with an increased Th17 response in Vogt-Koyanagi-Harada disease. *Invest. Ophthalmol. Vis. Sci.* **2012**, *53*, 4668–4675.

© 2013 by the authors; licensee MDPI, Basel, Switzerland. This article is an open access article distributed under the terms and conditions of the Creative Commons Attribution license (http://creativecommons.org/licenses/by/3.0/).

Mutagenesis vol. 28 no. 1 pp. 7–14, 2013
Advance Access publication 17 September 2012
doi:10.1093/mutage/ges043

UVB irradiation changes genotoxic potential of nonylphenolpolyethoxylates—remarkable generation of γ-H2AX with degradation of chemical structure

Tatsushi Toyooka, Toru Kubota and Yuko Ibuki*

Institute for Environmental Sciences, University of Shizuoka, 52-1, Yada, Suruga-ku, Shizuoka-shi, Shizuoka 422-8526, Japan

*To whom correspondence should be addressed. Tel: +81 54 264 5799; Fax: +81 54 264 5799; E-mail: ibuki@u-shizuoka-ken. ac.jp

Received on February 23, 2012; revised on June 1, 2012; accepted on June 14, 2012

Nonylphenolpolyethoxylates (NPEOs) are non-ionic surfactants widely used for industrial and household purposes. In actual environments, NPEOs can be biodegraded, but the products are reported to be more persistent and toxic than the parent compounds. NPEOs are also exposed to sunlight and degraded. Studies on the photodegradation of NPEOs have focused mainly on chemical changes after exposure to light. Toxic changes of photodegraded products correlating to the chemical changes are not completely understood. In this study, we examined the genotoxicity of UVB-irradiated NPEOs having ethylene oxide units 15 and 70 in a human breast adenocarcinoma cell line, MCF-7, based on the phosphorylation of histone H2AX (γ-H2AX), a sensitive marker for DNA damage. We clarified that UVB irradiation drastically changed the genotoxic potential of NPEOs: NPEO(15)'s ability to generate γ-H2AX was significantly reduced, whereas non-genotoxic NPEO(70) became able to generate γ-H2AX. Flow cytometric analysis showed that the γ-H2AX generated by UVB-irradiated NPEO(70) was produced independent of cell cycle phases. In addition, its production involved the activation of ATM or DNA-PK, a general signalling pathway in response to DNA double strand breaks. High-performance liquid chromatography analysis indicated that the formation of NPEO intermediates with a short side-chain like NPEO(15) was the cause of the γ-H2AX generation. This study suggests the importance of taking the genotoxicity of photodegraded intermediates into consideration when conducting risk assessments of environmental pollutants.

Introduction

Nonylphenolpolyethoxylates [NPEO(n), where n is the number of ethylene oxide (EO) units] belong to a group of non-ionic surfactants widely used in industrial, agricultural and household products (1). They have entered the environment via industrial effluents and human sewage as a result of their widespread usage. In actual environments, NPEOs can be biodegraded and the products including nonylphenol and short-chain NPEOs were reported to be more persistent and toxic than their parent compounds. These compounds are frequently identified as major contaminants in natural, waste and even drinking water (1–4).

In addition to biodegradation, photodegradation of NPEOs occurs in the environment. Of the various spectral bands [ultraviolet (UV), visible and infrared] in sunlight, UV rays play an important role in photodegradation. The UV spectrum can be divided into three based on wavelength: UVA (320–400 nm), UVB (280–320 nm) and UVC (200–280 nm). UVC and some UVB are absorbed in the stratospheric ozone layer, whereas UVA and most UVB reach the earth's surface. UVB photons contain the highest energy. Consequently, UVB radiation has the potential to contribute to photodegradation of chemical compounds present in the environment (5,6).

Although the chemical changes of NPEOs after exposure to sunlight have been studied (7,8), studies on toxic changes correlated with the photodegradation are rare. We have previously reported that UVB irradiation induced the degradation of NPEOs and caused toxic change depending on the shortening of EO units (9). Considering the cytotoxicity of photodegraded NPEOs, a determination of genotoxicity, highly correlated with carcinogenesis, would be needed for further risk assessments. However, toxicological studies of NPEOs have been mainly focused on endocrine-disrupting effects in aquatic organisms (10,11) and studies concerning the genotoxic effects of NPEOs, especially photodegraded NPEOs, in mammalian cells are completely lacking.

In eukaryotes, DNA is packaged into nucleosomes, the core of which is an octameric particle consisting of two each of the class H2A, H2B, H3 and H4 histones. H2AX is a minor component of histone H2A. Phosphorylation of histone H2AX (γ-H2AX) was originally identified as an early event after the direct formation of DNA double strand breaks (DSBs) by ionising radiation (12). However, the generation of γ-H2AX is now considered to occur also after the indirect formation of DSBs caused by the collision of the replication forks at sites of DNA damage including oxidative bases, DNA adducts, single strand breaks (SSBs) and cross-linking, and the repair of such damage (13,14). We previously reported that γ-H2AX was generated following the exposure of cells to various suspected DNA-damaging agents including several environmental chemicals and pharmacological agents (15–20). In addition to the advantage that γ-H2AX can be detected in response to many types of DNA damage, we and other researchers are convinced that γ-H2AX provides a considerably more sensitive and convenient measurement of DNA damage than other techniques such as pulse-field gel electrophoresis and comet assays (13,14,19,20). Therefore, focusing on γ-H2AX as a genotoxic marker is good way to identify the genotoxic potential of photodegraded NPEOs.

More recently, we elucidated the genotoxic potential of NPEO(n) having various EO units (n = 0–70) in a human breast adenocarcinoma cell line, MCF-7, based on γ-H2AX (21). The generation of γ-H2AX was strongly dependent on the number of EO units, that is, a significant amount of γ-H2AX was produced on treatment with NPEOs having fewer EO units (n = 0–15), whereas NPEOs with longer side chains like NPEO(70) attenuated the ability to generate γ-H2AX.

In this study, we examined the genotoxic change of NPEO(15) and NPEO(70) after exposure to UVB based on the generation of γ-H2AX. This is the first attempt to clarify the correlation of genotoxic changes of NPEOs with degradation of chemical structure after exposure to UV. Our results provide important information on the risk assessment of NPEOs present in the environment.

© The Author 2012. Published by Oxford University Press on behalf of the UK Environmental Mutagen Society.
All rights reserved. For permissions, please e-mail: journals.permissions@oup.com.

Materials and methods

NPEOs and UVB irradiation

NPEO(*n*) (*n* = 15 and 70) were kindly provided by NOF Co., Japan. They were dissolved in water at a stock concentration of 100 mM, and stored at 4°C until use. The molecular structures of the NPEOs are shown in Supplementary Figure 1 (available at *Mutagenesis* Online). NPEO (10 mM) solutions were prepared by diluting appropriate volumes of stock solutions with water in a glass dish 15 mm in diameter and 10 mm in height. To avoid evaporation, the glass dish was sealed with UV-transmittable film (DURA SEAL™: Diversified Biotech, Dedham, MA, USA). A UVB lamp (HP-30LM; Atto Co., Japan) with a 280–320 nm emission and a maximum peak of 312 nm was used for irradiation. The fluence was simultaneously measured and integrated using a radiometer (ATV-3W; Atto, Japan) with a 312 nm detector that was placed at the same distance as the glass dish from the UVB source. The approximate irradiance at the sample level was 2.0 mW/cm^2. It takes about 12 h for 100 J/cm^2 of irradiation.

Cells and culture conditions

The human breast adenocarcinoma cell line MCF-7 (provided by Japanese Collection of Research Bioresources, Japan) was maintained in Dulbecco's modified Eagle's medium (DMEM) supplemented with 10% foetal bovine serum and 100 U/ml of penicillin/streptomycin at 37°C in an atmosphere of 5% CO_2. All experiments were performed with exponentially growing cells. As the estrogenic effects of NPEOs were first identified in MCF-7 cell line (22), we used it in this study.

Cell survival after treatment with UVB-irradiated NPEOs

Cells grown on 35-mm culture dishes were treated with UVB-irradiated NPEOs (100–500 μM) for 24 h. The cells were washed with phosphate-buffered saline (PBS), trypsinised and suspended in DMEM. They were mixed with Trypan blue solution (0.3%) (1:1), and at least 400 cells were counted under a microscope. Dead cells had as a distinctive blue colour.

Immunofluorescence staining for detection of γ-H2AX

The cells treated with UVB-irradiated NPEOs in Lab-Tek chamber slides (NalgeNunc, IL, USA) were immediately fixed in 2% paraformaldehyde for 30 min at room temperature and then in 100% methanol for 20 min at −20°C. Fixed cells were immersed in buffer containing 100 mM Tris-HCl, 50 mM EDTA, and 0.5% Triton X-100 for 20 min at room temperature for better permealisation, and blocked with 1% bovine serum albumin (BSA) for 30 min at 37°C. Cells were incubated with a primary antibody against phospho-H2AX

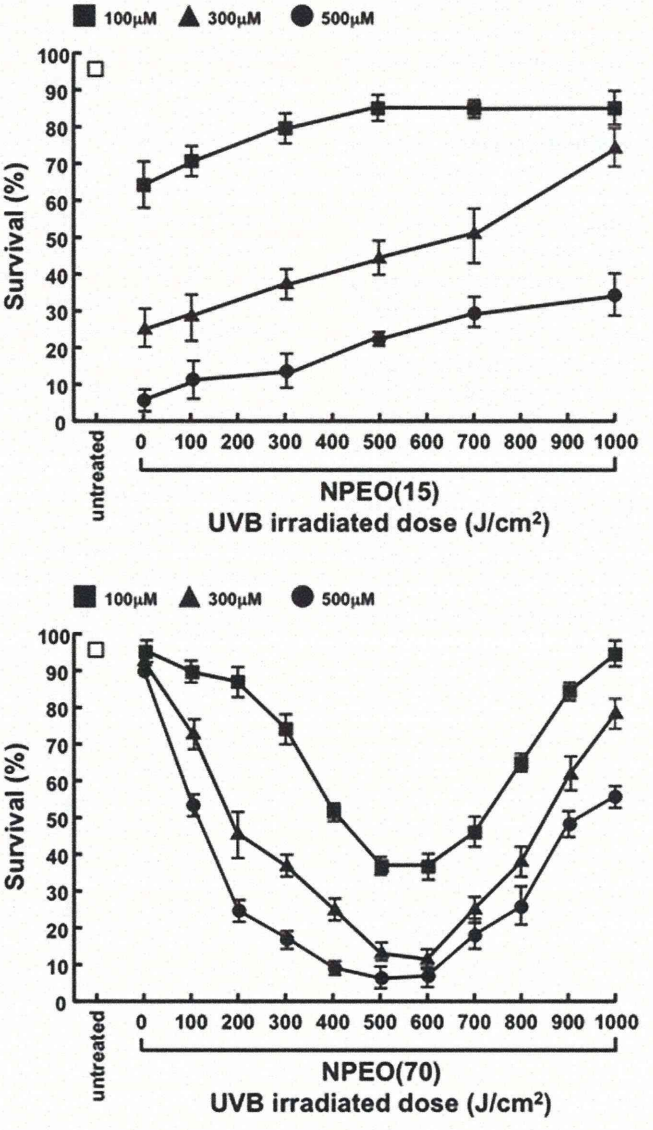

Fig. 1. Cytotoxicity of NPEOs irradiated with UVB. NPEO(15) and NPEO(70) were irradiated with UVB (100–1000 J/cm^2). Cell survival after treatment with UVB-irradiated NPEO(15) and NPEO(70) at concentrations ranging from 100 to 500 μM for 24 h was determined by Trypan blue exclusion assay. Values are the mean ± SD (*n* = 5).

(mouse monoclonal; Millipore, Bedford, MA, USA; 1:200) for 2 h, then with a secondary antibody conjugated with fluorescein isothiocyanate (FITC; Jackson Immuno Research Laboratories, PA, USA). To confirm the distribution of foci, the nucleus was stained with propidium iodide (PI; 20 μg/ml). Images were acquired on a fluorescence microscope (BX51, Olympus, Japan).

Western blot analysis of γ-H2AX

The cells treated with UVB-irradiated NPEOs were lysed in lysis buffer [50 mM Tris (pH 8.0), 5 mM EDTA, 150 mM NaCl, 0.5% Nonidet P-40 and 1 mM phenylmethylsulfonylfluoride (PMSF)]. The samples were separated by 12.5% SDS-PAGE, and blotted onto polyvinylidine fluoride (PVDF) membranes. After blocking with 1% non-fat milk, the membranes were incubated overnight at 4°C with a primary antibody against phospho-H2AX (rabbit polyclonal; 1:1000) or actin (Santa Cruz Biotechnology, CA, 1:1000), then with a secondary antibody conjugated with horseradish peroxidase (Jackson Immuno Research Laboratories, PA, USA) for 1 h. The bands of γ-H2AX were visualised with an enhanced chemiluminescence detection kit (GE Healthcare Ltd., UK).

Flow cytometric analysis of γ-H2AX and cell cycle distribution

The cells treated with UVB-irradiated NPEOs were fixed in ice-cold 70% ethanol and kept at −20°C for at least 2 h. The fixed cells were centrifuged at 2000 r.p.m. for 5 min and washed twice with PBS. They were resuspended in PBS containing 0.2% triton X-100 and 1% BSA (BSA-T-PBS) and kept at room temperature for 15 min. Cells were incubated with phospho-H2AX (mouse monoclonal; 1:200) for 1 h, then with a secondary antibody conjugated with FITC (1:200; Jackson Immuno Research Laboratories, PA, USA) for 1 h in BSA-T-PBS. After the immunoreaction, the cells were resuspended in BSA-T-PBS containing 1 μg/ml RNase A. PI (10 μg/ml) was added prior to the measurement for cell cycle analysis. The fluorescence intensity of FITC and PI was determined using flow cytometry (FCM; FACS CANTTM II; Becton Dickinson, Franklin Lakes, NJ, USA). At least 10,000 cells per sample were analysed.

Detection of DSBs

DSBs were detected with a biased sinusoidal field gel electrophoresis (BSFGE) system (Atto, Japan). The cells treated with UVB-irradiated NPEOs were solidified in 1% low-melting agarose. The agarose plugs were treated with proteinase K (0.5 mg/ml) and ribonuclease A (1 mg/ml), and electrophoresed in a 0.8% agarose gel. The gel was visualised by staining with ethidium bromide.

Flow cytometric detection of intracellular ROS

The intracellular generation of reactive oxygen species (ROS) in NPEO and H_2O_2-treated cells was investigated using 6-carboxy-2,7′-diclorodihydrofluorescein diacetate, di(acetoxymethyl ester) (DCFH-DA) (Molecular Probes, Eugene, OR, USA). Cells treated with NPEOs irradiated with UVB or H_2O_2 were incubated in the presence of 10 μM of DCFH-DA for 1 h. The fluorescence intensity of DCFH-DA inside the cells was determined by FCM.

HPLC analysis of NPEOs

In the high-performance liquid chromatography (HPLC) analysis (LC-10A, Shimazu, Japan), NPEOs were detected by monitoring UV absorbance at 275 nm (flow: 1.0 ml/min at 25°C). Ten microlitres of UVB-irradiated NPEOs dissolved in 30% acetonitrile (10 mM) were injected. A silica column [Shim-pack CLC-CIL (6.00 mm ID × 15 cm)] was used for all separations. The mobile phase solvent A was 30% acetonitrile. Solvent B was 80% acetonitrile. Elution was carried out with a linear gradient from 100% A to 100% B over 30 min.

Results

Cytotoxicity of NPEOs irradiated with UVB

Our previous study showed that the cytotoxicity of NPEOs was strongly dependent on the number of EO units using three kinds of cell lines (9). Also in MCF-7, NPEO(15) having a short side chain showed remarkable cytotoxicity, whereas no cytotoxic effect was observed for NPEO(70) having a long side chain (Figure 1). UVB irradiation decreased the cytotoxicity of NPEO(15) in a dose-dependent manner. Conversely, NPEO(70) gradually became cytotoxic on exposure to UVB up to around 500–600 J/cm^2, and thereafter gradually recovered (600–1000 J/cm^2).

Generation of γ-H2AX after treatment with UVB-irradiated NPEOs

We recently showed that NPEO(10), not NPEO(70), possessed genotoxic ability, using γ-H2AX, a marker of DNA damage (21). Since NPEO(70) was made cytotoxic by UVB irradiation (9), we next examined whether irradiation could change the genotoxic effect of NPEO(70) in MCF-7 cells. Cells were treated with 300 μM of UVB-irradiated NPEO(70) for 4 h. Images of immunofluorescence staining for γ-H2AX after the treatment are presented in Figure 2a and 2b. Characteristic foci of γ-H2AX distributed in the nucleus were clearly detected (Figure 2a). The patterns of γ-H2AX in cells treated with UVB (0,100, 300, 500, 700 and 1000 J/cm^2)-irradiated NPEO(70) are shown in Figure 2b. UVB-irradiated NPEO(70) generated γ-H2AX for increasing doses which led to a maximum induction at 500 J/cm^2, then higher doses of irradiation (700 and 1000 J/cm^2) attenuated the ability to generate γ-H2AX. The numbers of foci per nucleus also increased depending on the UVB-irradiated dose up to 500 J/cm^2 (data not shown). The γ-H2AX generated by NPEOs was confirmed in detail by western blotting (Figure 2c). The maximum generation of γ-H2AX was observed in NPEO(70) irradiated with around 500 J/cm^2 of UVB, consistent with the result of immunofluorescence staining. The generation of γ-H2AX by UVB-irradiated NPEO(70) was also observed in other cell line (Supplementary Figure 2, available at *Mutagenesis* Online). Since the generation of γ-H2AX is attributed to the formation of DSBs, DSBs induced by treatment with NPEO(70) (300 μM) for 4 h were detected by BSFGE (Figure 2d). UVB-irradiated NPEO(70) caused DNA migration, the extent of which was dependent on the irradiated dose, well consistent with the results of immunofluorescence staining and western blotting for γ-H2AX.

The generation of γ-H2AX by NPEO(15) was clearly attenuated by UVB irradiation, the extent of which was dependent on the irradiated dose of UVB (Figure 2e). Attenuated formation of DSBs by UVB irradiation was also confirmed by BSFGE (Figure 2f), consistent with the result of western blotting (Figure 2e). These results were also consistent with the data on cell survival in Figure 1.

Detailed analysis of γ-H2AX after treatment with UVB-irradiated NPEO(70)

Generation of γ-H2AX was observed very soon (15 min) after treatment with 300 μM of UVB (500 J/cm^2)-irradiated NPEO(70) and increased time-dependently (Figure 3a). γ-H2AX could be detected from a concentration of 100 μM, and increased depending on the concentration (Figure 3b). Similar results were also obtained in the detection of DSBs by BSFGE (Supplementary Figure 3, available at *Mutagenesis* Online).

Figure 3c shows the relationship between the generation of γ-H2AX and cell cycle distribution after treatment with UVB-irradiated NPEO(70) (300 μM) for 4 h. There are two ways in which γ-H2AX is generated (23). γ-H2AX production independent of the cell cycle is attributable to direct DSBs caused by DNA-damaging agents like ionising radiation (24). On the other hand, the high levels of γ-H2AX mainly in S-phase cells reflect DSBs resulting from the collapse of replication forks upon collision with primary DNA lesions formed

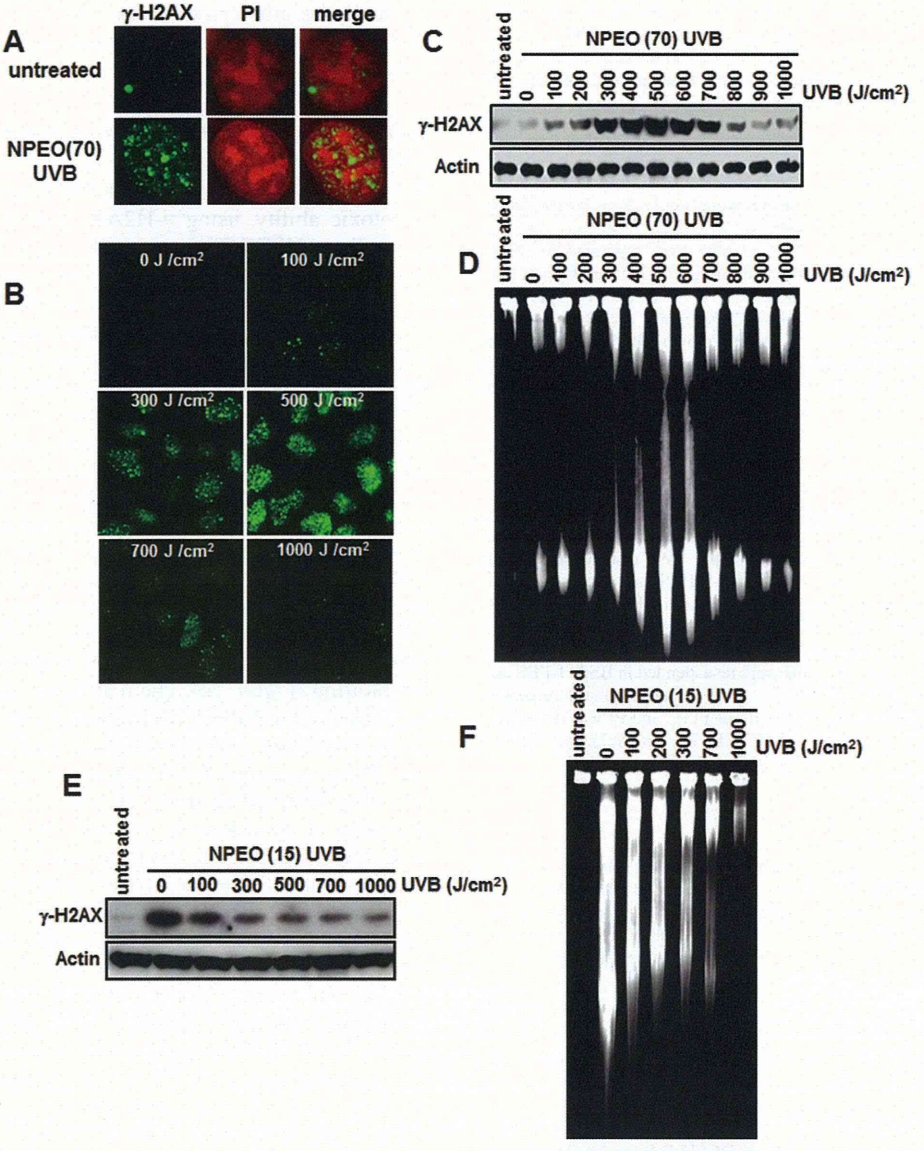

Fig. 2. Generation of γ-H2AX after treatment with UVB-irradiated NPEOs. (a) Magnified images of γ-H2AX foci produced by treatment with UVB (500 J/cm²)-irradiated NPEO(70) (300 μM) for 4 h. Nuclei were stained with PI. (b) Whole-cell image after treatment with UVB-irradiated NPEO(70) (300 μM). (c) Western blotting for detection of γ-H2AX after treatment with UVB-irradiated NPEO(70) (300 μM) for 4 h. Actin was used as a standard for the equal loading of proteins for SDS-PAGE. (d) Detection of DSBs after treatment with UVB-irradiated NPEO(70) (300 μM) for 4 h by BSFGE. (e) Western blotting for detection of γ-H2AX after treatment with UVB-irradiated NPEO(15) (300 μM). (f) Detection of DSBs after treatment with UVB-irradiated NPEO(15) (300 μM) for 4 h by BSFGE. All experiments were repeated two or three times.

by DNA-damaging agents like UV radiation (23). FCM histograms showed that the generation of γ-H2AX was not changed by treatment with NPEO(70) and augmented by UVB-irradiated NPEO(70). γ-H2AX-PI dot plots revealed that the increased fluorescence intensity of γ-H2AX occurred in all cell phases. These results suggested that UVB-irradiated NPEO(70) generated DSBs directly in all cell phases.

As histone H2AX has been considered a substrate of ATM and DNA-PK, DSBs-responsible-molecules (13,25), their inhibitors, wortmannin and caffeine, were added during the treatment with UVB-irradiated NPEO(70). The generation of γ-H2AX was clearly attenuated by both inhibitors (Figure 3d), indicating that γ-H2AX production by UVB-irradiated NPEO(70) was caused by ATM or DNA-PK activation based on DSBs.

Involvement of ROS in the generation of γ-H2AX by NPEO(70) irradiated with UVB

Since there was a report that nonylphenol generated oxidative DNA damage in calf thymus DNA after irradiation (26), we investigated the contribution of ROS to the generation of γ-H2AX by UVB-irradiated NPEO(70). Intracellular ROS levels after treatment with UVB (500 J/cm²)-irradiated NPEO(70) (300 μM) or H_2O_2 (3 mM) for 4 h were examined using a fluorescence ROS probe, DCFH-DA. Although the treatment with UVB-irradiated NPEO(70) produced ROS, the amount was quite small as compared with the treatment with H_2O_2 (Figure 4a). Figure 4b shows the generation of γ-H2AX after treatment with UVB-irradiated NPEO(70) (300 μM) or H_2O_2 (3 mM) for 4 h in the presence of an antioxidant,

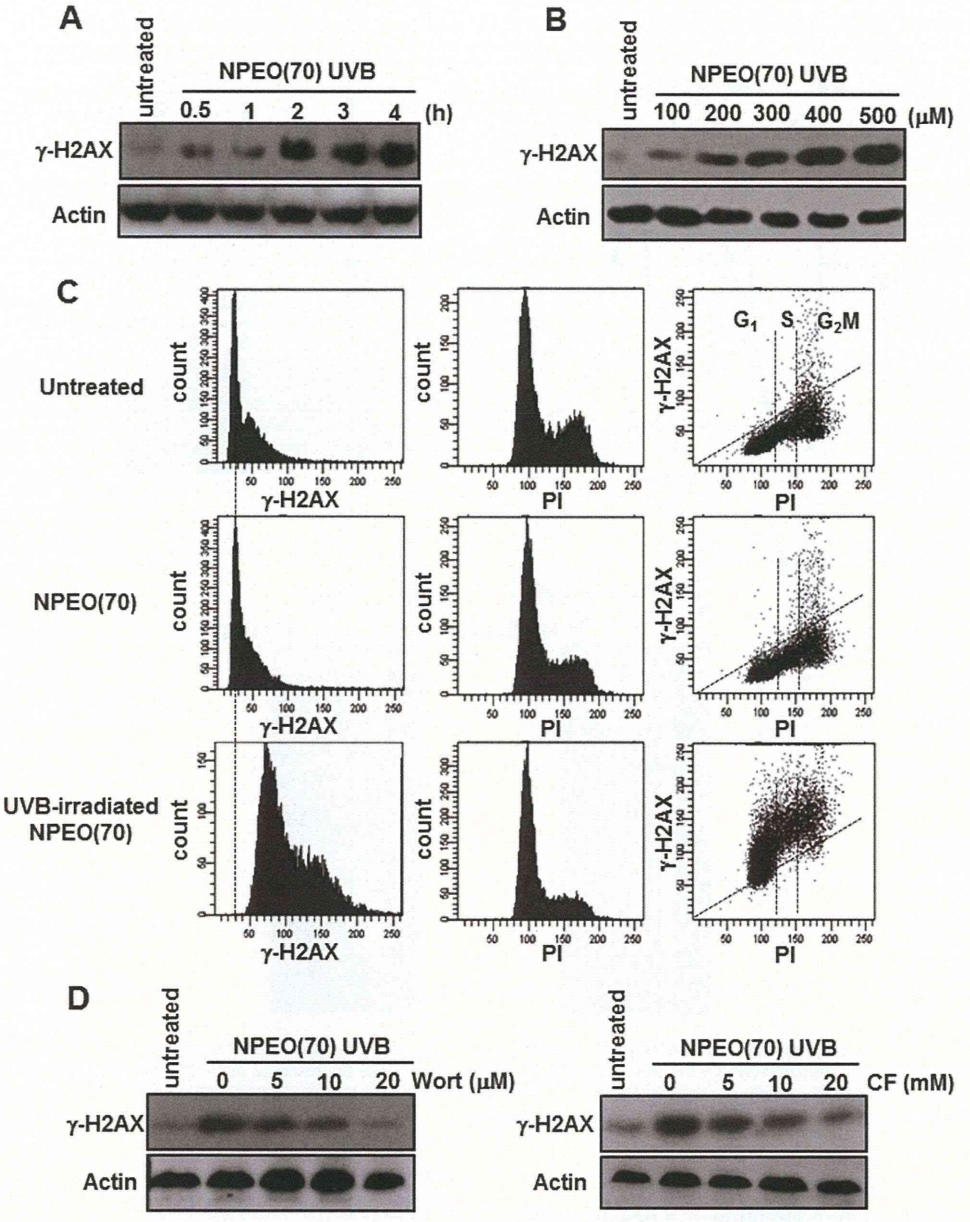

Fig. 3. Generation of γ-H2AX after treatment with UVB-irradiated NPEO(70). (a) Cells were treated with UVB (500 J/cm^2)-irradiated NPEO(70) (300 μM) for the period indicated (0.5–4 h). (b) Cells were treated with UVB (500 J/cm^2)-irradiated NPEO(70) (100–500 μM) for 4 h. Actin was used as a standard for the equal loading of proteins for SDS-PAGE. (c) Cells treated with NPEO(70) or UVB (500 J/cm^2)-irradiated NPEO(70) (300 μM) for 4 h were fixed and stained with antibody for γ-H2AX and PI. Left panels: histograms of γ-H2AX detected by immunofluorescence staining. Centre panels: cell cycle distribution analysed by PI staining. Right panels: dot blots of γ-H2AX and cell cycle phases (PI). (d) Cells were pretreated with inhibitors (wortmannin and caffeine) for 0.5 h, then treated with UVB-irradiated NPEO(70) (300 μM) for 4 h. All experiments were repeated two or three times with similar results.

N-acetylcystein (NAC). The amount of γ-H2AX generated by NPEO(70) irradiated with UVB was attenuated slightly in the presence of NAC, whereas γ-H2AX generated by H_2O_2 was completely suppressed. Similar results were also obtained in the detection of DSBs by BSFGE (Figure 4c). These results suggested that ROS was not the main causal factor in the generation of γ-H2AX by NPEO(70) irradiated with UVB.

HPLC analysis of NPEOs irradiated with UVB

We carried out an HPLC analysis of UVB-irradiated NPEO(15) and NPEO(70) to obtain information about the relationship between the chemical structure and genotoxicity of NPEOs. The original peak of NPEO(70) disappeared depending on the dose of UVB irradiation, and a new peak was identified at a similar retention time to NPEO(15) (Figure 5a). The newly generated peak reached a maximum at 500 J/cm^2, and any further irradiation led to its disappearance. In the case of NPEO(15), the original peak disappeared depending on the irradiation dose (Figure 5b). These results were well consistent with the results regarding cytotoxicity in Figure 1 and the generation of γ-H2AX in Figure 2.